NeuroImage 55 (2011) 176–184

Contents lists available at ScienceDirect

NeuroImage

journal homepage: www.elsevier.com/locate/ynimg

Quantitative analysis of hemodynamic and metabolic changes in subcortical vascular dementia using simultaneous near-infrared spectroscopy and fMRI measurements

Sungho Tak [a], Soo Jin Yoon [b], Jaeduck Jang [a], Kwangsun Yoo [a], Yong Jeong [a,*], Jong Chul Ye [a,*]

[a] Department of Bio and Brain Engineering, KAIST, Daejeon, Republic of Korea
[b] Department of Neurology, Eulji University College of Medicine, Daejeon, Republic of Korea

ARTICLE INFO

Article history:
Received 13 August 2010
Revised 25 October 2010
Accepted 13 November 2010
Available online 20 November 2010

Keywords:
Near-infrared spectroscopy
Neurovascular coupling
Functional magnetic resonance imaging
Subcortical vascular dementia

ABSTRACT

Subcortical vascular dementia (SVD) is a form of vascular dementia from small vessel disease with white matter lesions and lacunes. We hypothesized that hemodynamic and metabolic changes in the cortex during a simple motor task may reflect the impaired neurovascular coupling in SVD. We used fMRI and near-infrared spectroscopy (NIRS) simultaneously, which together provided multiple hemodynamic responses as well as a robust estimation of the cerebral metabolic rate of oxygen ($CMRO_2$). During the task periods, the oxy-hemoglobin, total-hemoglobin, blood oxygenation level-dependent (BOLD) response, cerebral blood flow (CBF), and $CMRO_2$ decreased statistically significantly in the primary motor and somatosensory cortices of SVD patients, whereas the oxygen extraction fraction increased when compared with controls. Notably, the flow–metabolism coupling ratio, n representing the ratio of oxygen supply to its utilization, showed a robust reduction in the SVD patient group ($n_{Control} = 1.99 \pm 0.23$; $n_{SVD} = 1.08 \pm 0.24$), which implies a loss of metabolic reserve. These results support the pathological small vessel compromise, including an increased vessel stiffness, impaired vascular reactivity, and impaired neurovascular coupling in SVD. In conclusion, simultaneous measurement by NIRS and fMRI can reveal various hemodynamic and metabolic changes and may be used for as an early detection or monitoring of SVD.

Introduction

Subcortical vascular dementia (SVD) is a form of vascular dementia that results from small vessel disease that leads hypoperfusion and ischemia to white matter and subcortical structures (Román et al., 2002; Chui, 2001). The typical symptoms of SVD are slowness in motor performance as well as in cognitive processing, which result from early impairment of attention and executive function (Román, 1987). There are two known major pathophysiological mechanisms in SVD: lacunes due to arteriolar occlusion and widespread incomplete infarction of deep white matter due to hypoperfusion (Enolund et al., 1987). Practically, the two mechanisms can occur together. It can be conjectured that a prolonged mismatch between oxygen supply and its utilization may be attributed to the pathophysiological mechanism of SVD due to relative hypoxic insults. This is supported by recent evidences showing that mechanisms such as impaired neurovascular coupling or vasomotor reactivity may contribute to the pathogenesis of SVD (Schroeter et al., 2007; Bar et al., 2007). Therefore, quantitative measurement of these parameters may help in understanding of the pathophysiology and diagnosis of SVD.

Many neuroimaging studies have identified a correlation with either hemodynamic or metabolic changes and cognitive deficits in SVD patients, depending on the specific imaging modality, such as positron emission tomography (PET) and single-photon emission computed tomography (SPECT)(Yao et al., 1990; Kuwabara et al., 1995; Tohgi et al., 1991; Yoshikawa et al., 2003). However, to elucidate the pathophysiological mechanism more precisely, both hemodynamic and metabolic changes should be considered simultaneously.

Near-infrared spectroscopy (NIRS) can monitor the concentration changes in oxy-hemoglobin (HbO), deoxy-hemoglobin (HbR), and total-hemoglobin (HbT) by measuring the absorption changes of near-infrared light through the intact skull. Due to the great sensitivity of NIRS to the microvasculature (Liu et al., 1995), NIRS may be more applicable to investigations of hemodynamic changes in patients with SVD. However, to the best of our knowledge, there have been only a few studies that used NIRS on SVD patients. One recent study using NIRS showed early deoxygenation after the onset of a stimulus along with a delayed restoration of the hemodynamic response in patients with cerebral microangiopathy (Schroeter et al., 2007). We have recently developed a method to estimate the changes in cerebral blood flow (CBF) and cerebral metabolic rate of oxygen ($CMRO_2$) using the hemodynamic responses of NIRS and functional

* Corresponding authors. J.C. Ye is to be contacted at Bio Imaging and Signal Processing Lab., Department of Bio and Brain Engineering, KAIST, 335 Gwahak-ro, Yuseong-gu, Daejeon 305-701, Republic of Korea. Fax: +82 42 350 4310. Y. Jeong, Laboratory for Cognitive Neuroscience and NeuroImaging, Department of Bio and Brain Engineering, KAIST, 335 Gwahak-ro, Yuseong-gu, Daejeon 305-701, Republic of Korea. Fax: +82 42 350 4380.
E-mail addresses: yong@kaist.ac.kr (Y. Jeong), jong.ye@kaist.ac.kr (J.C. Ye).

1053-8119/$ – see front matter © 2010 Elsevier Inc. All rights reserved.
doi:10.1016/j.neuroimage.2010.11.046

magnetic resonance imaging (fMRI) (Tak et al., 2010). As this method does not require an additional hypercapnia process, the controversial assumption of $CMRO_2$ invariance during hypercapnia (Kliefoth et al., 1979; Jones et al., 2005) is not necessary. Furthermore, multiple unknown parameters (including the baseline hemoglobin concentration) of which the physiological ranges are uncertain in SVD are readily optimized. This may promise more accurate estimations of the CBF, $CMRO_2$, flow–metabolism coupling ratio, and oxygen extraction fraction (OEF).

Even though CBF and $CMRO_2$ signals measured from NIRS come from cortices rather than subcortices, recent studies show additional hypoperfusion and even thinning of the cortex in SVD patients (Seo et al., 2010; Fein et al., 2000; Pantel et al., 2000). In SVD, it is more reasonable to think that hypoperfusion occurs both at the subcortex and cortex. Evidence of cortical hypoperfusion or hypometabolism is supported by many functional imaging studies. PET (Yao et al., 1990; Kuwabara et al., 1995) and SPECT(Tohgi et al., 1991; Yoshikawa et al., 2003) studies observed a decrease in cerebral blood flow (CBF) and cerebral metabolic rate of oxygen ($CMRO_2$) of the cortex in patients with SVD. Specifically, Yao et al. (1990) found that CBF and $CMRO_2$ were significantly reduced in the grey matter including the parietal (73% of control values), frontal (74–80%), and temporal (74–83%) cortices in patients with Binswanger type vascular dementia where no structural abnormality was detected. These findings were also accompanied by decreases of CBF and $CMRO_2$ in the white matter (54–77% of control values).

Therefore, using simultaneous recording of NIRS and fMRI, we aimed to clarify the changes in various vascular responses, including hemoglobin oxidation, the blood oxygenation level-dependent (BOLD) response, the CBF, the $CMRO_2$, the flow–metabolism coupling ratio, and the OEF in the primary motor and somatosensory cortices of SVD patients while they performed a repeated hand grip task. We hypothesized that different magnitudes or time delays of hemodynamic and metabolic signals that result from impaired flow–metabolism coupling may appear in the motor cortex during a task, which implies the existence of impaired neurovascular coupling of SVD.

Materials and methods

Subject

Six patients with SVD and 6 age-matched healthy controls were recruited. Demographies and the clinical information of the subjects are summarized in Table 1. The diagnosis of SVD was based on a modification of the National Institute of Neurological Disorders and Stroke and the Association Internationale pour la Recherche et l'Enseignement en Neurosciences (NINDS-AIREN) criteria for probable vascular dementia (Erkinjuntti et al., 2000). Brain MRI were performed in 5 SVD patients, and brain CT was performed in one. Their brain images were compatible with the imaging criteria for SVD (Erkinjuntti et al., 2000; Román et al., 2002). Healthy controls showed neither a history of neurological and psychiatric disorders nor any impairment of their daily activities. They were normal in neurologic evaluation. There was no significant abnormality in MRI, either. To evaluate the cognitive function, the Korean version of Mini-Mental State Examination (K-MMSE) (Kang et al., 1997) was done in all subjects. After all subjects and their caregivers were given instructions concerning the experimental environment, and the operating mode of NIRS and fMRI, signed informed consent forms were obtained. This study was approved by the Institutional Review Board of the Korea Advanced Institute of Science and Technology (KAIST).

Table 1
Clinical characteristics of healthy controls and the patients with subcortical vascular dementia. Values are the mean ± standard error of the mean (SEM). *Significant difference according to the Mann–Whitney *U* test ($p<0.05$). Abbreviations: SVD, subcortical vascular dementia; K-MMSE, Korean mini-mental state examination; CDR, clinical dementia rating scale; WM, white matter.

Variables	Healthy controls	SVD patients
Number of subjects	6	6
Sex (male/female)	3/3	2/4
Age (years)	76.5 ± 3.1	73.3 ± 1.2
*K-MMSE	27.2 ± 0.4	19 ± 1.5
Disease duration (years)	–	2.7 ± 0.7
CDR	–	1.0 ± 0.2
*WM volume change (cc)	2.0 ± 0.9	37.2 ± 6.1

Data acquisition

We measured the hemodynamic signals using NIRS and fMRI simultaneously. Detailed system specifications are as follows: a continuous wave NIRS instrument (Oxymon MK III, Artinis, The Netherlands) was used to measure the optical density variations, which result from the changes in hemoglobin concentrations. The NIRS system emitted 781 nm and 856 nm laser lights at each source fiber. The fiber length was 10 m to connect the optodes in the MR scanner to the NIRS system in the MR control room. The sampling frequency was 10 Hz. The NIRS system had 24 channels with eight sources and four detectors. The distance between a source and a detector was 3.5 cm. An optode holder cap was attached to the scalp around the left fronto-parietal areas to cover the primary motor, somatosensory, and supplementary motor cortices. For spatial registration of the NIRS channels to the Montreal Neurological Institute (MNI) standard space, MR marker capsules were placed on the optode holder cap. The locations of the marker capsules were used to elicit the relationship between the real coordinates and MNI coordinates using the algorithm of Horn et al. (1987).

Using a 3.0-T MR scanner (FORTE, ISOL Technology, Republic of Korea), the blood oxygenation level-dependent (BOLD) changes and structural MR images were obtained. Specifically, the BOLD response was measured using the echo planar imaging (EPI) sequence (repetition time [TR]= 3000ms, echo-time [TE]= 35ms, flip angle = 80°, 35 axial slices, slice thickness = 4 ms, matrix size = $64 \times 64mm^2$, field of view [FOV] = $220 \times 220mm^2$). In order to detect the white matter lesions and lacunar infarcts for a diagnosis of SVD, T2-weighted fast spin echo multi-slice (FSEMS) images (TR= 5000ms, TE= 64ms, flip angle = 80°, 35 axial slices, slice thickness = 4 ms, matrix size = $192 \times 256mm^2$, FOV = $192 \times 220mm^2$) and T1-weighted fluid-attenuated inversion recovery (FLAIR) images (TR= 2800ms, TE= 16ms, flip angle = 80°, 35 axial slices, slice thickness = 4 ms, matrix size = $192 \times 256mm^2$, FOV = $192 \times 220mm^2$) were also acquired.

Task protocols

A repeated right hand grip task was used to detect differences in the hemodynamic and metabolic changes between SVD patients and healthy controls. Instructions were presented visually. When the word “Go” appeared, the subjects were to perform a simple flexion and extension of their right fingers repeatedly. When the word “Stop” appeared, the subjects were to stop moving and stare at a fixed point to avoid eye and head movements. Since patients' attention and executive functions can be easily interfered with, subjects were monitored by an operator inside the MR scanner room to confirm an accurate task and to stop unnecessary movements. If the patients could not understand a visual instruction, a vocal instruction was alternatively given by an operator. We used block design sequences that consisted of 21 s of task and 30 s of rest in one cycle. The full experimental run consisted of 42 s of rest, followed by ten task and rest cycles. The total recording time was 552 s.

Data analysis

Calculation of hemoglobin concentration changes

The modified Beer–Lambert law (Cope and Delpy, 1988) describing optical attenuation in a highly scattering medium such as biological tissue provides a relationship between the changes in optical density and chromophore concentration. According to the modified Beer–Lambert law, the optical density variation $\Delta\phi(r,s;\lambda,t)$ (unitless quantity) at time t can be described as

$$\Delta\phi(r,s;\lambda,t) = -ln\frac{U(r,s;\lambda,t)}{U_o(r,s;\lambda)} = d(r)l(r)\sum_{i=1}^{N_c} a_i(\lambda)\Delta c_i(r;t), \quad (1)$$

where (r,s) denotes the detector and source position, λ is the wavelength of the laser source, N_c is the number of chromophores, $U(r,s;\lambda,t)$ denotes the measured photon flux at time t, $U_o(r,s;\lambda)$ denotes the initial photon flux, $\Delta c_i(r,t)$ denotes the changes in ith chromophore concentration, $a_i(\lambda)$ is the extinction coefficient of the ith chromophore at wavelength λ, $l(r)$[mm] is the distance between the source and detector, and $d(r)$ is the differential path-length factor (DPF) accounting for the increased distance that light travels from the source to the detector due to scattering and absorption effects at the position r. Assuming that HbO and HbR are the major two chromophores in the wavelength range of 600 to 900 nm, we can rewrite Eq. (1) as

$$\Delta\phi(r,s;\lambda,t) = d(r)l(r)[a_{HbO}(\lambda)\Delta c_{HbO}(r;t) + a_{HbR}(\lambda)\Delta c_{HbR}(r;t)], \quad (2)$$

where $\Delta c_{HbO}(r;t)$ and $\Delta c_{HbR}(r;t)$ denote the HbO and HbR concentration changes, and $a_{HbO}(\lambda)$ and $a_{HbR}(\lambda)$ denote the extinction coefficients of HbO and HbR at wavelength λ, respectively. The optical density changes measured at two wavelengths (λ_1 and λ_2) are then given by the following matrix formulation:

$$\begin{bmatrix}\Delta\phi(r,s;\lambda_1,t)\\ \Delta\phi(r,s;\lambda_2,t)\end{bmatrix} = d(r)l(r)\begin{bmatrix}a_{HbO}(\lambda_1) a_{HbR}(\lambda_1)\\ a_{HbO}(\lambda_2) a_{HbR}(\lambda_2)\end{bmatrix}\begin{bmatrix}\Delta c_{HbO}(r;t)\\ \Delta c_{HbR}(r;t)\end{bmatrix}. \quad (3)$$

Here, we assume that $d(r)$ is the same at both wavelengths. By multiplying the inverse matrix of extinction coefficients, and inverse of $d(r)$ and $l(r)$ with Eq. (3), the concentration changes of HbO andHbR, $\Delta c_{HbO}(r;t)$ and $\Delta c_{HbR}(r;t)$ are finally determined by

$$\begin{bmatrix}\Delta c_{HbO}(r;t)\\ \Delta c_{HbR}(r;t)\end{bmatrix} = \frac{1}{d(r)l(r)}\begin{bmatrix}a_{HbO}(\lambda_1) & a_{HbR}(\lambda_1)\\ a_{HbO}(\lambda_2) & a_{HbR}(\lambda_2)\end{bmatrix}^{-1}\begin{bmatrix}\Delta\phi(r,s;\lambda_1,t)\\ \Delta\phi(r,s;\lambda_2,t)\end{bmatrix}. \quad (4)$$

Estimation of cerebral blood flow and metabolic rate of oxygen

Several methods can determine $CMRO_2$ changes using fMRI (Davis et al., 1998; Hoge et al., 1999) or NIRS (Boas et al., 2003; Mayhew et al., 2001) measurements. The main rationale for estimating metabolic parameter from hemodynamic measurement is that the HbR concentration at venous compartment is output function of oxygen supply (CBF) and oxygen utilization ($CMRO_2$). However, these approaches require a separate hypercapnia process or have the potential to incur bias in many assumed model parameters. To overcome the drawbacks of conventional approaches, the authors recently developed a novel method to estimate $CMRO_2$ changes without hypercapnia using simultaneous NIRS and fMRI measurements. We briefly describe this method here (see more details in Tak et al., 2010).

According to the BOLD biophysical model (Davis et al., 1998; Hoge et al., 1999), the relative $CMRO_2$–CBF coupling ratio is given by

$$\frac{rCMRO_2(t)}{rCBF(t)} = rCBV(t)^{-1/\beta}\left(1-\frac{1}{H}\cdot\frac{\Delta BOLD(t)}{BOLD_0}\right)^{1/\beta}. \quad (5)$$

Here, H is the hypercapnia calibration parameter; β is a constant ranging from 1 to 2; the subscript '0' denotes the baseline value; $rCMRO_2(t)$ and $rCBF(t)$ denote the relative $CMRO_2$ and CBF to their respective baselines.

Using the Fick's law (Hoge et al., 1999), which describes the ratio of $CMRO_2$ to CBF as the HbR concentration within the venous compartment of a constant unit volume element of tissue, the following expression can be obtained:

$$\frac{rCMRO_2(t)}{rCBF(t)} = \frac{[HbR(t)]_v}{[HbR]_{v,0}} = \frac{rHbR_v(t)}{rCBV_v(t)}, \quad (6)$$

where the subscript 'v' denotes the venous vasculature, the subscript '0' denotes the baseline value, and $rHbR(t)$ and $rCBV(t)$ denote the relative HbR and CBV to their respective baselines. Since the NIRS measurements are intrinsically from well-mixed vascular compartments, under the assumption that the quantities in the venous vasculature are proportional to those in the total vascular compartments ($HbR_{v,0} = r_1 HbR_0$, $\Delta HbR_v = r_2 DeltaHbR$, $CBV_{v,0} = r_3 CBV_0$, $\Delta CBV_v = r_4 \Delta CBV$), Eq. (6) can be rewritten as follows (Boas et al., 2003; Mayhew et al., 2001):

$$\frac{rCMRO_2(t)}{rCBF(t)} = \frac{1+\gamma_r(\Delta HbR(t)/HbR_0)}{1+\gamma_v(\Delta CBV(t)/CBV_0)}, \quad (7)$$

where the unknown constants γ_r and γ_v are given by

$$\gamma_r = \frac{r_2}{r_1} = \frac{\Delta HbR_v/\Delta HbR}{HbR_{v,0}/HbR_0} \quad \gamma_v = \frac{r_4}{r_3} = \frac{\Delta CBV_v/\Delta CBV}{CBV_{v,0}/CBV_0}. \quad (8)$$

Due to the simultaneous recording of NIRS and fMRI, the relative $CMRO_2$–CBF coupling ratio derived from BOLD and NIRS biophysical models should be identical. Hence, using Eq. (5) and Eq. (7) give:

$$rCBV(t)^{-1/\beta}\left(1-\frac{1}{H}\cdot\frac{\Delta BOLD(t)}{BOLD_0}\right)^{1/\beta} = \frac{1+\gamma_r(\Delta HbR(t)/HbR_0)}{1+\gamma_v(\Delta CBV(t)/CBV_0)}. \quad (9)$$

To estimate unknown model parameters including $H, \beta, \gamma_r, \gamma_v, CBV_0, HbR_0$, the regression problem is converted as follows:

$$\min_{H,\beta,\gamma_r,\gamma_v,CBV_0,HbR_0}\sum_{i=1}^{N}\left\|\frac{\Delta BOLD(t_i)}{BOLD_0} - \xi(t_i)\right\|_2, \quad (10)$$

where

$$\xi(t_i) = H\left(1-\left(1+\gamma_0\frac{\Delta CBV(t_i)}{CBV_0}\right)\left(\frac{1+\gamma_r(\Delta HbR(t_i)/HbR_0)}{1+\gamma_v(\Delta CBV(t_i)/CBV_0)}\right)^{\beta}\right).$$

Here, $\|\cdot\|_2$ denotes the l_2 norm, and $\gamma_0 = \gamma_v$ because the CBV in the BOLD model mainly comes from the venous compartment (Wu et al., 2002). The fitting problem in Eq. (9) was converted to Eq. (10) so as to use NIRS measured oxygen species as covariates to fit the BOLD response. Due to the same cost value given by the infinite number of (HbR_0, γ_r) and (CBV_0, γ_v) pairs, we estimate HbR_0/γ_r and CBV_0/γ_v as the single independent variables η_r and η_v, respectively.

To calculate model parameters less sensitive to the signal-to-noise ratio of NIRS and BOLD measurements, a wavelet-based adaptive averaging method is used to estimate the hemodynamic response function (HRF) of NIRS and BOLD measurements, rather than simple averaging of measurements across experimental blocks. The average HbO, HbR, HbT, and BOLD time series are then estimated by convolving each HRF with the relevant experimental paradigms. A cost function for HRF estimation based on the minimum description length (MDL) principle for NIRS (Rissanen, 1978; Jang et al., 2009) and the Schwartz information criterion (SIC) principle for BOLD (Schwarz, 1978; Meyer, 2003) is as follows:

$$c(n_0) = \frac{N}{2}log\,\hat{\sigma}^2(n_0) + L(n_0), \quad (11)$$

where

$$L(n_0) = \begin{cases} \frac{3}{2} n_0 \log M : & \text{NIRS} \\ \frac{1}{2} n_0 \log M : & \text{BOLD} \end{cases}$$

and

$$\hat{\sigma}^2(n_0) = \frac{1}{N} \left\| y^{(i)} - \left(a\theta_j[0]\left(\Phi\left(2^{-J}t\right) * s\right) + \sum_{j=J_0}^{J} \sum_{k=0}^{2^{-j}M-1} d\theta_j[k]\left(\psi\left(2^{-j}t-k\right) * s\right) \right) \right\|_2^2.$$

Here, $y^{(i)}$ denotes the measurement at the ith channel, s is the input paradigm response, ψ is the wavelet, $\Phi(t)$ is the scaling function associated with a multiresolution analysis, J is the maximum level of wavelet decomposition, J_0 is the finest scale determining the smoothness of the trend, n_0 denotes the number of non-zero coefficients in the wavelet decomposition, N is the number of samples for the NIRS or BOLD time series, and M is the number of samples within one block. To find the optimal parameter n_0 for Eq. (11), LASSO regression (Tibshirani, 1996) is employed.

At this point, using the optimal model parameters, the relative $CMRO_2$–CBF coupling ratio $\frac{\widehat{rCMRO_2}(t)}{rCBF(t)}$ can be estimated by either the NIRS or the BOLD biophysical model. Here, the relative oxygen extraction fraction (rOEF) is identical to the relative $CMRO_2$–CBF coupling ratio:

$$OEF(t) = \frac{CMRO_2(t)}{CBF(t)} \cdot \frac{1}{C_a}$$

$$rOEF(t) = \frac{OEF(t)}{OEF_0} = \frac{CMRO_2(t)/CBF}{CMRO_{2,0}/CBF_0} = \frac{rCMRO_2(t)}{rCBF(t)}, \quad (12)$$

where C_a denotes the arterial oxygen concentration. In the simultaneous recording of NIRS and fMRI, CBF is not measured directly but is instead estimated using the model of CBF–CBV relationship (Grubb et al., 1974; Buxton et al., 1998). For example, using the model of Grubb et al. (1974), which describes the steady-state relationship between CBF and CBV, the relative CBF can be calculated as follows:

$$rCBF(t) = rCBV(t)^{1/\alpha}. \quad (13)$$

In this equation, a value of $\alpha = 0.38$ is typically employed. The relative $CMRO_2$ is then calculated by multiplying the relative $CMRO_2$–CBF coupling ratio and CBF:

$$rCMRO_2(t) = \frac{\widehat{rCMRO_2}(t)}{rCBF(t)} \cdot \widehat{rCBF}(t), \quad (14)$$

where $\frac{\widehat{rCMRO_2}(t)}{rCBF(t)}$ denotes the estimated relative coupling ratio and $\widehat{rCBF}(t)$ is the estimated relative CBF.

The algorithm to estimate $CMRO_2$–CBF from simultaneous NIRS and fMRI has been already implemented in a NIRS-SPM software package and can be downloaded from the authors' webpage (http://bisp.kaist.ac.kr/NIRS-SPM).

Quantification of white matter hyperintensity

The quantification of white matter hyperintensity (WMH) was performed semi-automatically using the MRICro program (http://www.cabiatl.com/mricro/mricro.html). On FLAIR images, regions of interests (ROI) that have higher intensity than a certain level of intensity threshold were drawn automatically. The threshold level was determined by the level that covers all the regions with white matter hyperintensity. Then noises and ROIs other than white matter were erased. Only the areas in subcortical regions were selected and double checked by two neurologists (Y. Jeong and S. J. Yoon) as to whether they were true lesions. The volume of white matter hyperintensity was automatically calculated by MRICro.

Data processing

The overall process of analyzing the NIRS and fMRI data was performed using the software package NIRS-SPM (http://bisp.kaist.ac.kr/NIRS-SPM, Ye et al. (2009)). Using the modified Beer–Lambert law in Eq. (1), the concentration changes in HbO and HbR were obtained from NIRS measurements. After eliciting the MNI coordinates of NIRS channels from the algorithm of Horn et al. (1987), the BOLD signals at the voxels that corresponds to the location of NIRS channels were extracted. To remove the noise from the NIRS and BOLD time series, Gaussian smoothing with a full width at half maximum (FWHM) of 2 s was applied. The wavelet-MDL based detrending algorithm (Jang et al., 2009) was used to eliminate unknown global trends such as breathing, subject movement, or instrumental instability. For more robust estimation of average NIRS and BOLD time series across the experimental blocks, a wavelet-based adaptive averaging method was used in estimating the HRF (Tak et al., 2010). After obtaining the HRFs of each response, the average HbO, HbR, HbT, and BOLD response values were estimated by convolving these values with the experimental paradigms. To investigate the different behaviors of the hemodynamic and metabolic changes in motor functions, we selected ROIs as the primary motor and somatosensory cortices using the WFR PickAtlas toolbox (www.ansir.wfubmc.edu).

By solving the regression problem in Eq. (10), time series of relative $CMRO_2$–CBF coupling ratio and model parameters for the channels located in the ROI were readily estimated. The physiological ranges of model parameters including H, η_r, and η_v were explored primarily in healthy young adults (less than 34 years old) in previous studies (Chiarelli et al., 2007; Torricelli et al., 2001; Boas et al., 2003). However, to our knowledge, the physiological ranges of those model parameters for SVD are not well established. So, we expanded the search region of the model parameters for SVD patients and healthy old adults twice as much as those for healthy young adults. To ensure the accurate estimation of H, η_r, and η_v, the following rejection criteria was used: if on the specific channel the coefficient of determination (R^2) was less than 0.81 (i.e., $R<0.9$) for the linear fit of the relative $CMRO_2$–CBF coupling ratio of NIRS versus that of the BOLD biophysical models, the estimated model parameters were discarded. On average, more channels in SVD patients were rejected from further channel-wise analysis compared to those of controls (control 1 ± 0.4, SVD 1.8 ± 0.5), as shown in Table 2. Recall that the BOLD(Davis et al., 1998; Hoge et al., 1999) and NIRS biophysical models (Boas et al., 2003; Mayhew et al., 2001) determining the $CMRO_2$ changes have been derived using healthy subjects. So, we conjecture that the impaired neurovascular and metabolic coupling in SVD patients probably may make it more difficult to fit the relative $CMRO_2$–CBF coupling ratio from both biophysical models, so the rejection ratio may increase. Finally, the relative CBF and relative $CMRO_2$ values were calculated using Eq. (13) and Eq. (14), respectively. Fig. 1 shows a flow chart describing the procedures from the measurements to the wavelet-based adaptive average estimation and the CBF/$CMRO_2$ estimation.

To statistically compare the difference in hemodynamic and metabolic responses between the SVD and control groups, the channel-wise analysis was performed. Average numbers of channels used in statistical analysis were 3.5 ± 0.6 and 2.3 ± 0.4 regarding the individuals of controls and SVD, respectively (see Table 2). Two-tailed unpaired Student's t-tests (ST) was performed, and equality of variance was also tested using Levene's test (LV) (Levene, 1960). Since the sample size of this study is small, the normality assumption of t-test may not be held. Therefore, we also performed the Mann–Whitney U test (MW), a non-parametric test that does not assume that sample differences are normally distributed or the variances of the two populations are equal (Mann and Whitney, 1947). The

Table 2
Average number of channel used in the channel-wise analysis between SVD and controls. The channels located in the region of interest (ROI), primary motor and somatosensory cortices, were selected regarding each individual. If on the specific channel the coefficient of determination (R^2) was less than 0.81 for the linear fit of the relative $CMRO_2$–CBF coupling ratio from NIRS versus that of the BOLD biophysical models, those channels were discarded for further statistical analysis. Values are the mean ± standard error of the mean (SEM).

Variables	Average number of channels	
	Healthy controls	SVD patients
Located within ROI	4.5 ± 0.4	4.2 ± 0.4
Rejected	1 ± 0.4	1.8 ± 0.5
Used for further analysis	3.5 ± 0.6	2.3 ± 0.4

corresponding p values for the Student's t-test and Mann–Whitney U test are denoted by p_{ST} and p_{MW}, respectively.

Results

The K-MMSE scores of the SVD group were significantly lower than those of the healthy controls (HC) (HC 27.2 ± 0.4, SVD 19.0 ± 1.5; $p_{MW} = 0.005$). White matter changes in the SVD group were significantly higher than those in the healthy controls (HC 2.0 ± 0.9cc, SVD 37.2 ± 6.1cc; $p_{MW} = 0.005$), as shown in Table 1. Two groups were not different in age and sex ratio. Statistical significance was determined by a p-value of less than 0.05.

The group-average time series of hemodynamic and metabolic changes in SVD patients and healthy controls are shown in Fig. 2. During task periods, the amplitudes of hemodynamic and metabolic changes in SVD patients showed a decrease except for the changes of HbR. The solid black line denotes the period of the hand grip task. For a quantitative analysis, we calculated the mean value of each response during task periods (Table 3) and graphically represented them, as shown in Fig. 3. The changes of HbO in the SVD patients were significantly reduced compared with the controls ($HbO_{HC} = 0.35 \pm 0.05\mu M$, $HbO_{SVD} = 0.09 \pm 0.05\mu M$; $p_{MW} = 0.004$; $p_{ST} = 0.002$). Also, the HbT was markedly decreased in SVD patients ($HbT_{HC} = 0.19 \pm 0.06\mu M$, $HbT_{SVD} = -0.01 \pm 0.06\mu M$; $p_{MW} = 0.004$; $p_{ST} = 0.02$). However, differences in the HbR responses were not observed ($HbR_{HC} = -0.13 \pm 0.03\mu M$, $HbR_{SVD} = -0.12 \pm 0.03\mu M$; $p_{MW} = 0.7$; $p_{ST} = 0.8$). Fractional BOLD changes in SVD were significantly decreased compared to the controls ($BOLD_{HC} = 102.72 \pm 14.5\%$, $BOLD_{SVD} = 51.05 \pm 11.5\%$; $p_{MW} = 0.007$; $p_{ST} = 0.02$). The variance was not statistically different between SVD and control regarding HbO, HbT, HbR, and BOLD (see Table 3).

In the SVD patients, fractional changes in CBF and $CMRO_2$ were decreased remarkably to 19.7% of the control group ($CBF_{HC} = 26.68 \pm 5.48\%$, $CBF_{SVD} = 5.25 \pm 4.39\%$; $p_{MW} = 0.006$; $p_{ST} = 0.01$) and 4.3% of the control group ($CMRO_{2,HC} = 10.06 \pm 3.18\%$, $CMRO_{2,SVD} = 0.43 \pm 2.87\%$; $p_{MW} = 0.02$; $p_{ST} = 0.05$), respectively. From the fractional CBF and $CMRO_2$ changes, the flow–metabolism coupling ratio, n, can be calculated as follows:

$$n = \frac{\Delta CBF / CBF_0}{\Delta CMRO_2 / CMRO_{2,0}}. \quad (15)$$

The flow–metabolism coupling ratios of the SVD patients and the controls were 1.08 ± 0.24 and 1.99 ± 0.23, respectively, which show the significant decrease of n in SVD group ($p_{MW} = 0.003$; $p_{ST} = 0.01$). Furthermore, an increase in the OEF was observed in SVD patients ($OEF_{HC} = -10.81 \pm 1.94\%$, $OEF_{SVD} = -3.77 \pm 1.19\%$; $p_{MW} = 0.004$; $p_{ST} = 0.01$). Again, the equality of variance was not statistically different between SVD and control regarding CBF, $CMRO_2$, n, and OEF (see Table 3).

During post-stimulus periods, the recovery rate of hemodynamic and metabolic responses generally slowed in SVD patients, as shown in Fig. 2. We estimated the time-to-fall (T_f) of the signals, this being the time taken to fall to the baseline value. The T_f values of HbO and CBF in SVD patients (9.8 s and 8.8 s, respectively) were longer than those of the controls (9.1 s and 7.2 s, respectively).

Correlation analyses were performed relating the results of the hemodynamic and metabolic changes to the K-MMSE scores and the volume of white matter hyperintensities (Table 4). The K-MMSE scores were correlated significantly with HbO, BOLD, CBF, and OEF. Furthermore, the volume of white matter hyperintensities had significantly correlative trends with HbT, CBF, $CMRO_2$, and the flow–metabolism coupling ratio.

To clarify whether the difference in cortical activation pattern of SVD may contribute to the differences in hemodynamic and metabolic responses, we illustrate the fMRI group activation pattern ($p < 0.001$, uncorrected) for SVD and controls in Fig. 4. In both groups, the activated regions were tightly localized on the primary motor cortex. This result supports that the difference in cortical activation pattern during task between SVDs and controls is not significant and the reduction of hemodynamic and metabolic changes in SVD is mainly from the impaired neurovascular couping. This coincides with previous studies showing that although the hemodynamic response during stimulation is decreased, the neuronal activation is preserved in cerebral microangiopathy (Rossini et al., 2004; Schroeter et al., 2007).

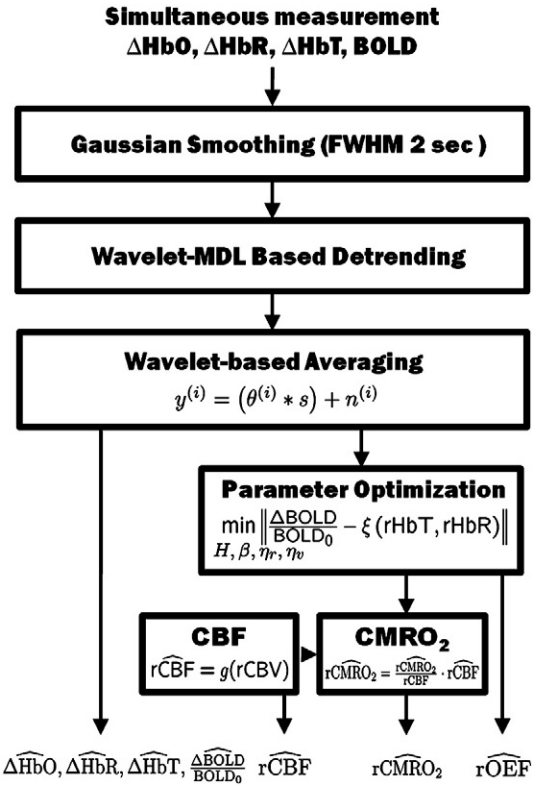

Fig. 1. Schematics describing procedures from near-infrared spectroscopy (NIRS) and blood oxygenation level-dependent (BOLD) measurements for the cerebral blood flow (CBF) and cerebral metabolic rate of oxygen ($CMRO_2$) estimation. In the step of wavelet-based adaptive averaging, $y^{(i)}$ denotes the measurement at the ith channel, $\theta^{(i)}$ is the hemodynamic response function, and s is the input experimental protocol. In the parameter estimation step, ξ(rHbT, rHbR) denotes the biophysical model of fractional BOLD changes.

Discussion

Numerous studies of SVD patients have observed a reduction of CBF or $CMRO_2$ in the frontal lobes during a "resting" state (Yoshikawa et al., 2003; Yao et al., 1990; De Reuck et al., 1998; Yang et al., 2002).

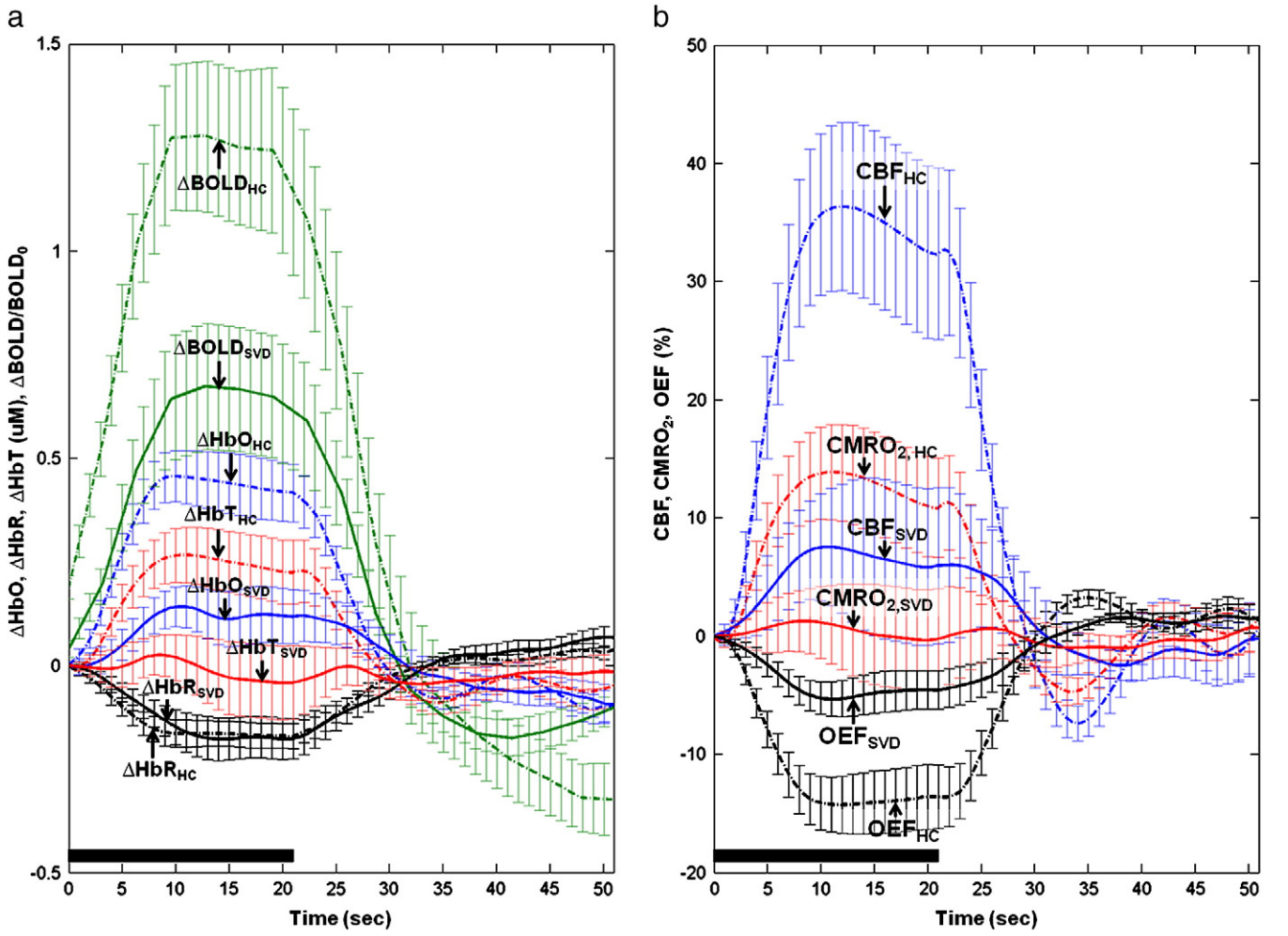

Fig. 2. Group-average time courses of (a) oxy-hemoglobin (HbO), deoxy-hemoglobin (HbR), total-hemoglobin (HbT), and fractional blood oxygenation level-dependent (BOLD) changes; (b) fractional cerebral blood flow (CBF), cerebral metabolic rate of oxygen ($CMRO_2$), oxygen extraction fraction (OEF) changes in subcortical vascular dementia (SVD), and healthy control (HC) groups. The solid black line indicates the hand grip task period. The error bar denotes the standard error of the mean (SEM) across the subjects at each time point. The subscripts HC and SVD denote the group responses from healthy control and SVD, respectively. The region of interest was selected as the primary motor and somatosensory cortices.

However, few studies have investigated different vascular responses of SVD patients during an "activation" state. We note that the main clinical manifestations of SVD are slow behavior and delayed information processing due to a deficit of fronto-subcortical connections. Therefore, we hypothesized that during neural activation, hemodynamic and metabolic changes in SVD patients may clearly reflect impaired neurovascular coupling, and vasomotor reactivity, as during a resting state. Therefore, we studied the hemodynamic and metabolic changes during a simple motor task.

We measured the cerebral hemodynamic and metabolic changes in SVD patients using simultaneous NIRS and fMRI measurement. One of the advantages of our method is that we can estimate $CMRO_2$ changes without hypercapnia challenging. In this study, we used a simple motor task instead of sensory or other cognitive tasks to evoke hemodynamic changes in the cortex. The hand grip task was used to assess vascular responses instead of other cognitive, motor, or sensory stimulation tasks for several reasons. Considering that NIRS can measure hemodynamic changes only at the dorsal surface of the brain, only the tasks that are known to activate the dorsal surface are possible. One possible task was the *n*-back test (Smith et al., 1998); however, patients with cognitive impairment would show variable performance levels in this task. This may lead to wide individual variation in brain activation not by cerebral hemodynamic changes but according to cognitive performance. A possible alternative was a repeated hand grip with close monitoring by an operator. Another reason to choose this motor task was that the patients with subcortical cognitive impairments frequently show pyramidal or extrapyramidal motor signs. These clinical features are often attributed to damage in the frontal–subcortical circuits; however, the primary motor cortex itself may also become injured from ischemia or may experience secondary injury after axonal injury.

We found cortical reduction of hemodynamic and metabolic responses in SVD patients. These findings were expected since the primary pathophysiology of SVD is the narrowing or occlusion of small vessels that cause hypoperfusion to their supplying areas. In SVD, the hypoperfusion often leads to lacunar infarcts in subcortical structures and ischemic white matter lesions (Román et al., 2002). However, the hemodynamic changes measured by NIRS and fMRI actually occurred in the cortex. Even though SVD is known as a disease of subcortical structures as its name indicates, there have been many reports on cortical changes in SVD. In patients with SVD, cortical hypoperfusion using SPECT (Yang et al., 2002), hypometabolism using FDG-PET, and cortical thinning have been reported (Seo et al., 2010; Fein et al., 2000; Pantel et al., 2000). The mechanism of cortical changes is not well understood yet; however, secondary neuronal degeneration by axonal injury may be attributed to cortical changes.

Table 3
Group-average hemodynamic and metabolic changes within the primary motor and somatosensory cortices during hand grip tasks for healthy controls and subcortical vascular dementia patients. Values are the mean ± standard error of the mean (SEM). *Statistical significance was determined by a *p*-value of less than 0.05. Abbreviations: SVD, subcortical vascular dementia; HbO, oxy-hemoglobin; HbR, deoxy-hemoglobin; HbT, total-hemoglobin; BOLD, blood oxygenation-level-dependent response; CBF, cerebral blood flow; $CMRO_2$, cerebral metabolic rate of oxygen; OEF, oxygen extraction fraction; LV, Levene's test; ST, two-tailed unpaired Student's *t*-test; MW, Mann–Whitney *U* test.

Variables	Group-average values		*p*-value		
	Control	SVD	MW	ST	LV
HbO changes (ΔHbO, μM,)	0.35 ± 0.05	0.09 ± 0.05	0.004*	0.002*	0.2
HbR changes (ΔHbR, μM)	−0.13 ± 0.03	−0.12 ± 0.03	0.7	0.8	0.7
HbT changes (ΔHbT, μM)	0.19 ± 0.06	−0.01 ± 0.06	0.004*	0.02*	0.8
BOLD changes ($\Delta BOLD/BOLD_0$, %)	102.72 ± 14.5	51.05 ± 11.5	0.007*	0.02*	0.3
CBF changes ($\Delta CBF/CBF_0$, %)	26.68 ± 5.48	5.25 ± 4.39	0.006*	0.01*	0.2
$CMRO_2$ changes ($\Delta CMRO_2/CMRO_{2,0}$, %)	10.06 ± 3.18	0.43 ± 2.87	0.02*	0.05*	0.3
OEF changes ($\Delta OEF/OEF_0$, %)	−10.81 ± 1.94	−3.77 ± 1.19	0.004*	0.01*	0.2
Coupling ratio, n $\left(\frac{\Delta CBF}{CBF_0} / \frac{\Delta CMRO_2}{CMRO_{2,0}}\right)$	1.99 ± 0.23	1.08 ± 0.24	0.003*	0.01*	0.7

Table 4
Correlation between hemodynamic/metabolic changes, K-MMSE, and WMH. **$p<0.01$, *$p<0.05$., Correlation coefficient *r* according to Pearson, two-tailed *p*-value. Abbreviations: K-MMSE, Korean mini-mental state examination; WMH, white matter hyperintensity; HbO, oxy-hemoglobin; HbR, deoxy-hemoglobin; HbT, total-hemoglobin; BOLD, blood oxygenation level-dependent response; CBF, cerebral blood flow; $CMRO_2$, cerebral metabolic rate of oxygen; OEF, oxygen extraction fraction; *n*, flow–metabolism coupling ratio.

Variables	K-MMSE	WMH
HbO	0.66*	−0.51
HbR	−0.39	−0.2
HbT	0.54	−0.76**
BOLD	0.66*	−0.41
CBF	0.64*	−0.58*
$CMRO_2$	0.52	−0.58*
OEF	−0.66*	0.52
n	0.56	−0.78**

The cortical injury can occur proximal to an injured axon (dying-back) or distally (Wallerian degeneration) (Ginsberg and Martin, 2002; Johnson and Cowey, 2000; Schallert et al., 1990).

Other mechanisms are also thought to contribute to decreased CBF and other parameters. Blood flow is mainly proportional to the systolic blood pressure and inversely proportional to blood viscosity. In the pathogenesis of SVD, arteriosclerosis can cause hyperviscosity (Caplan, 1995), which may lead to decreased CBF. Cerebral autoregulation allows a constant CBF to be maintained over a wide range of blood pressure readings (approximately 60 to 150 mm Hg). However, in SVD patients, the autoregulatory range becomes narrowed (Román et al., 2002) and vasoreactivity is severely impaired (De Reuck et al., 1999; Kuwabara et al., 1995). Thus, compromised autoregulatory reserve and vascular reserve are considered as additional factors resulting in the reduced CBF and $CMRO_2$ of SVD patients. This coincides with our finding that fractional changes of CBF and $CMRO_2$ in SVD patients were significantly reduced.

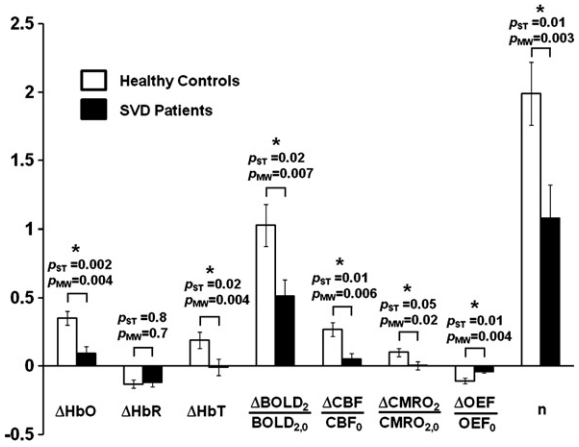

Fig. 3. Bar graphs representing mean values of hemodynamic and metabolic changes during hand grip task periods from subcortical vascular dementia (SVD, shaded bars) and healthy controls (open bars). Lines represent the standard error of the mean (SEM). The p_{ST} and p_{MW} denote the two-tailed unpaired Student's *t*-test and the Mann–Whitney *U* test, respectively. *Indicates the significant difference according to the *p*-value less than 0.05. Equality of variance was tested using Levene's test.

Interestingly, the fractional change of OEF in SVD patients increased to 34.9%, in addition to the decrease of CBF and $CMRO_2$. To compensate for the decreasing CBF, the OEF, representing the relationship between the CBF (i.e., oxygen supply) and $CMRO_2$ (i.e., oxygen utilization), should increase. However, if such compensation is not sufficient, the oxygen supply cannot meet the demand, thus the $CMRO_2$ decreases and there are relative ischemic insults to the supplying areas. Note that this increased OEF implies a loss of metabolic reserve (Heiss and Podreka, 1993) and may be one of the indicators for differentiating small vessel vascular dementia from large vessel vascular dementia (De Reuck et al., 1998, 1999). Specifically, De Reuck et al. (1998) showed that in patients with vascular dementia due to microangiopathy, the OEF was increased in all brain regions with a reduced CBF and $CMRO_2$, whereas in patients with vascular dementia due to large infarcts, the OEF was preserved with a decreased coupled CBF and $CMRO_2$.

Our study showed that the flow–metabolism coupling ratio, *n*, in SVD (1.08 ± 0.24) is significantly reduced compared to the healthy controls (1.99 ± 0.23). The fractional coupling ratio between the CBF and $CMRO_2$ for healthy controls is generally within the range of 2–4 (Boas et al., 2003; Hoge et al., 1999; Durduran et al., 2004; Sheth et al., 2004; Kastrup et al., 2002; Davis et al., 1998). The mechanism underlying the significant decrease of *n* in SVD can be explained as follows. Under normal conditions, an increase of CBF in over-proportion to that of $CMRO_2$ during activation is accompanied by a decreased of OEF, which implies a metabolic reserve. However, in SVD patients, the OEF should increase to compensate for the reduced CBF originating from microvasculature changes, such as increased vessel stiffness and compromised smooth muscle cells (Caplan, 1995; Román et al., 2002). Since the relationship between the OEF and the flow–metabolism coupling ratio is approximately inversely proportional, we can infer that an increased OEF leads to a decreased flow–metabolism coupling ratio. Hence, the flow–metabolism coupling ratio of approximately 1 in SVD patients clearly indicates that most of the oxygen supply is utilized, which implies a loss of metabolic reserve. The significant reduction of the coupling ratio in our study clearly supports the presence of compromised neurovascular coupling.

We detected a significant decrease of HbO and HbT in SVD patients. According to the close relationship between CBF and CBV (Eq. (13), Grubb et al. (1974)), the reduction of HbT proportional to the CBV (Villringer and Chance, 1997) can be interpreted as the hypoperfusion of SVD. In addition, because an oversupply of oxygen is not maintained in SVD ($\Delta CBF/\Delta CMRO_2 \approx 1$), HbO significantly decreases in SVD compared to healthy controls.

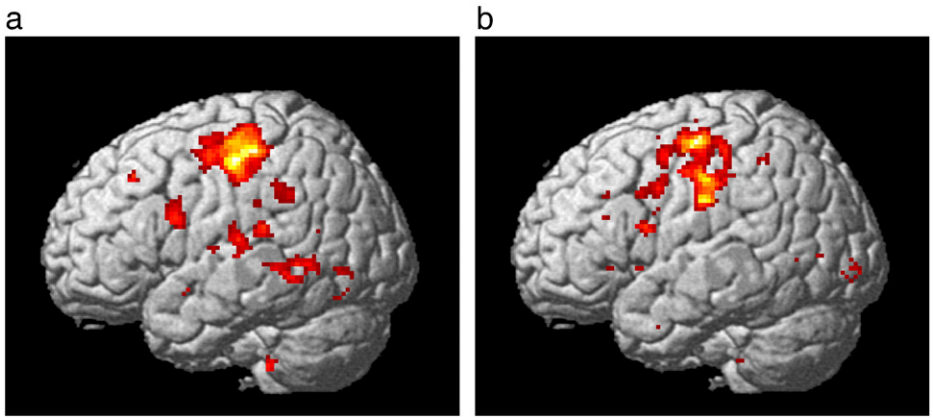

Fig. 4. Group activation found by BOLD measurements of (a) healthy controls and (b) SVD patients during the repeated right hand grip task ($p<0.001$, uncorrected). In both groups, the activated regions were consistent with the primary motor cortex, which is the main target region of this experiment.

From the experimental results of this study, the processes of impaired hemodynamic and metabolic responses were hypothesized, as shown in Fig. 5. More specifically, from multiple pathological changes in SVD, a significant reduction of CBF first occurred, which was accompanied by a slight increase of the OEF to compensate for the loss of the oxygen supply. However, if such compensation is not sufficient, the oxygen supply cannot meet the demand, thus the $CMRO_2$ will decrease and there will be relative ischemic insults to the supplying areas. Due to the close relationship between CBF and CBV (Eq. (13), Grubb et al. (1974)), CBV also significantly decreases, which is followed by a reduction of HbO. If the oxygen extraction factor increases sufficiently, HbR may not show significant differences against the reduced HbO (Schroeter et al., 2005). The BOLD signal has multiple sources of signal changes such as CBV and OEF (Davis et al., 1998). Consequently, a significant decrease of the BOLD response can be observed in the absence of changes in HbR.

In summary, using simultaneous NIRS and fMRI, we found a decreased CBF, $CMRO_2$, and flow–metabolism coupling ratio, along with an increased OEF in SVD patients, which may explain the underlying pathophysiology including hypoperfusion, hypometabolism, and impaired neurovascular coupling. One limitation of this study is a relatively small sample size. Hence, large-scale experiments may be required in the future to generalize the findings of this study.

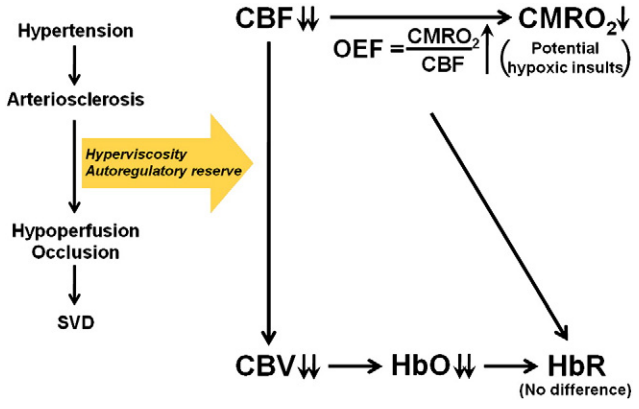

Fig. 5. Diagram of the hypothetical pathways of impaired neurovascular coupling in SVD patients. From multiple pathological changes in SVD, a significant reduction of CBF first occurred, which was accompanied by a slight increase of OEF to compensate for the loss of the oxygen supply. However, if such compensation is not sufficient, the oxygen supply cannot meet the demanding amount, thus the $CMRO_2$ will decrease and there will be relative ischemic insults to the supplying areas. Due to the close relationship between CBF and CBV (Eq. (**13**) (Grubb et al., 1974)), CBV also significantly decreases, which is followed by a reduction of HbO. If the oxygen extraction factor increases sufficiently, HbR may not show significant differences against the reduced HbO.

Acknowledgments

This study was supported by the Industrial Strategic Technology Program of the Ministry of Knowledge Economy (KI001889).

References

Bar, K., Boettger, M., Seidler, N., Mentzel, H., Terborg, C., Sauer, H., 2007. Influence of galantamine on vasomotor reactivity in Alzheimer's disease and vascular dementia due to cerebral microangiopathy. Stroke 38 (12), 3186–3192.
Boas, D., Strangman, G., Culver, J., Hoge, R., Jasdzewski, G., Poldrack, R., Rosen, B., Mandeville, J., 2003. Can the cerebral metabolic rate of oxygen be estimated with near-infrared spectroscopy? Phys. Med. Biol. 48 (15), 2405–2418.
Buxton, R., Wong, E., Frank, L., 1998. Dynamics of blood flow and oxygenation changes during brain activation: the balloon model. Magn. Reson. Med. 39, 855–864.
Caplan, L., 1995. Binswanger's disease–revisited. Neurology 45 (4), 626–633.
Chiarelli, P., Bulte, D., Gallichan, D., Piechnik, S., Wise, R., Jezzard, P., 2007. Flow–metabolism coupling in human visual, motor, and supplementary motor areas assessed by magnetic resonance imaging. Magn. Reson. Med. 57 (3), 538–547.
Chui, H., 2001. Dementia due to subcortical ischemic vascular disease. Clin. Cornerstone 3 (4), 40–51.
Cope, M., Delpy, D., 1988. System for long-term measurement of cerebral blood and tissue oxygenation on newborn infants by near infra-red transillumination. Med. Biol. Eng. Comput. 26 (3), 289–294.
Davis, T., Kwong, K., Weisskoff, R., Rosen, B., 1998. Calibrated functional MRI: mapping the dynamics of oxidative metabolism. Proc. Natl Acad. Sci. USA 95 (4), 1834–1839.
De Reuck, J., Decoo, D., Marchau, M., Santens, P., Lemahieu, I., Strijckmans, K., 1998. Positron emission tomography in vascular dementia. J. Neurol. Sci. 154 (1), 55–61.
De Reuck, J., Decoo, D., Hasenbroekx, M., Lamont, B., Santens, P., Goethals, P., Strijckmans, K., Lemahieu, I., 1999. Acetazolamide vasoreactivity in vascular dementia: a positron emission tomographic study. Eur. Neurol. 41 (1), 31–36.
Durduran, T., Yu, G., Burnett, M., Detre, J., Greenberg, J., Wang, J., Zhou, C., Yodh, A., 2004. Diffuse optical measurement of blood flow, blood oxygenation, and metabolism in a human brain during sensorimotor cortex activation. Opt. Lett. 29 (15), 1766–1768.
Enolund, E., Brun, A., Persson, B., 1987. Correlations between histopathologic white matter changes and proton MR relaxation times in dementia. Alzheimer Dis. Assoc. Disord. 1 (3), 156–170.
Erkinjuntti, T., Inzitari, D., Pantoni, L., Wallin, A., Scheltens, P., Rockwood, K., Roman, G., Chui, H., Desmond, D., 2000. Research criteria for subcortical vascular dementia in clinical trials. J. Neural Transm. Suppl. 59, 23–30.
Fein, G., Di Sclafani, V., Tanabe, J., Cardenas, V., Weiner, M., Jagust, W., Reed, B., Norman, D., Schuff, N., Kusdra, L., Greenfield, T., Chui, H., 2000. Hippocampal and cortical atrophy predict dementia in subcortical ischemic vascular disease. Neurology 55 (11), 1626–1635.
Ginsberg, S., Martin, L., 2002. Axonal transection in adult rat brain induces transsynaptic apoptosis and persistent atrophy of target neurons. J. Neurotrauma 19 (1), 99–109.
Grubb, R., Raichle, M., Eichling, J., Ter-pogossian, M., 1974. The effects of changes in $PaCO_2$ cerebral blood bolume, blood flow, and vascular mean transit time. Stroke 5 (5), 630–639.
Heiss, W., Podreka, I., 1993. Role of PET and SPECT in the assessment of ischemic cerebrovascular disease. Cerebrovasc. Brain Metab. Rev. 5 (4), 235–263.
Hoge, R., Atkinson, J., Gill, B., Crelier, G., Marrett, S., Pike, G., 1999. Investigation of BOLD signal dependence on cerebral blood flow and oxygen consumption: the deoxyhemoglobin dilution model. Magn. Reson. Med. 42 (5), 849–863.
Horn, B., et al., 1987. Closed-form solution of absolute orientation using unit quaternions. J. Opt. Soc. Am. A 4 (4), 629–642.

Jang, K., Tak, S., Jung, J., Jang, J., Jeong, Y., Ye, J., 2009. Wavelet minimum description length detrending for near-infrared spectroscopy. J. Biomed. Opt. 14 (3), 034004.
Johnson, H., Cowey, A., 2000. Transneuronal retrograde degeneration of retinal ganglion cells following restricted lesions of striate cortex in the monkey. Exp. Brain Res. 132 (2), 269–275.
Jones, M., Berwick, J., Hewson-Stoate, N., Gias, C., Mayhew, J., 2005. The effect of hypercapnia on the neural and hemodynamic responses to somatosensory stimulation. Neuroimage 27 (3), 609–623.
Kang, Y., Na, D., Hahn, S., 1997. A validity study on the Korean Mini-Mental State Examination (K-MMSE) in dementia patients. J. Korean Neurol. Assoc. 15 (2), 300–308.
Kastrup, A., Kruger, G., Neumann-Haefelin, T., Glover, G., Moseley, M., 2002. Changes of cerebral blood flow, oxygenation, and oxidative metabolism during graded motor activation. Neuroimage 15 (1), 74–82.
Kliefoth, A., Grurb Jr., R., Raichle, M., 1979. Depression of cerebral oxygen utilization by hypercapnia in the rhesus monkey. J. Neurochem. 32 (2), 661–663.
Kuwabara, Y., Ichiya, Y., Sasaki, M., Yoshida, T., Masuda, K., 1995. Time dependency of the acetazolamide effect on cerebral hemodynamics in patients with chronic occlusive cerebral arteries: early steal phenomenon demonstrated by [^{15}O] H_2O positron emission tomography. Stroke 26 (10), 1825–1829.
Levene, H., 1960. Robust tests for equality of variances. In: Olkin, I., Ghurye, S., Hoeffding, W., Madow, W., Mann, H. (Eds.), Contribution to Probability and Statistics. Stanford University Press, California, CA, pp. 278–292.
Liu, H., Boas, D., Zhang, Y., Yodh, A., Chance, B., 1995. Determination of optical properties and blood oxygenation in tissue using continuous NIR light. Phys. Med. Biol. 40, 1983–1993.
Mann, H., Whitney, D., 1947. On a test of whether one of two random variables is stochastically larger than the other. Ann. Math. Stat. 18 (1), 50–60.
Mayhew, J., Johnston, D., Berwick, J., Jones, M., Coffey, P., Zheng, Y., 2001. Erratum and addendum: spectroscopic analysis of neural activity in brain: increased oxygen consumption following activation of barrel cortex. Neuroimage 13, 540–543.
Meyer, F., 2003. Wavelet-based estimation of a semiparametric generalized linear model of fMRI time-series. IEEE Trans. Med. Imaging 22 (3), 315–322.
Pantel, J., Schroder, J., Essig, M., Jauss, M., Schneider, G., Eysenbach, K., Von Kummer, R., Baudendistel, K., Schad, L., Knopp, M., 2000. In vivo quantification of brain volumes in subcortical vascular dementia and Alzheimer's disease. An MRI-based study. Dement. Geriatr. Cogn. Disord. 9 (6), 309–316.
Rissanen, J., 1978. Modeling by shortest data description. Automatica 14 (5), 465–471.
Román, G., 1987. Senile dementia of the Binswanger type. A vascular form of dementia in the elderly. JAMA 258 (13), 1782–1788.
Román, G., Erkinjuntti, T., Wallin, A., Pantoni, L., Chui, H., 2002. Subcortical ischaemic vascular dementia. Lancet Neurol. 1 (7), 426–436.
Rossini, P., Altamura, C., Ferretti, A., Vernieri, F., Zappasodi, F., Caulo, M., Pizzella, V., Del Gratta, C., Romani, G., Tecchio, F., 2004. Does cerebrovascular disease affect the coupling between neuronal activity and local haemodynamics? Brain 127 (1), 99.
Schallert, T., Jones, T., Lindner, M., 1990. Multilevel transneuronal degeneration after brain damage. Behavioral events and effects of anticonvulsant gamma-aminobutyric acid-related drugs. Stroke 21 (11 Suppl), 143–146.
Schroeter, M., Bucheler, M., Preul, C., Scheid, R., Schmiedel, O., Guthke, T., Von Cramon, D., 2005. Spontaneous slow hemodynamic oscillations are impaired in cerebral microangiopathy. J. Cereb. Blood Flow Metab. 25 (12), 1675–1684.
Schroeter, M., Cutini, S., Wahl, M., Scheid, R., Yves von Cramon, D., 2007. Neurovascular coupling is impaired in cerebral microangiopathy-an event-related stroop study. Neuroimage 34 (1), 26–34.
Schwarz, G., 1978. Estimating the dimension of a model. Ann. Stat. 6 (2), 461–464.
Seo, S., Ahn, J., Yoon, U., Im, K., Lee, J., Kim, S., Ahn, H., Chin, J., Jeong, Y., Na, D., 2010. Cortical thinning in vascular mild cognitive impairment and vascular dementia of subcortical type. J. Neuroimaging 20 (1), 37–45.
Sheth, S., Nemoto, M., Guiou, M., Walker, M., Pouratian, N., Toga, A., 2004. Linear and nonlinear relationships between neuronal activity, oxygen metabolism, and hemodynamic responses. Neuron 42 (2), 347–355.
Smith, E., Jonides, J., Marshuetz, C., Koeppe, R., 1998. Components of verbal working memory: evidence from neuroimaging. Proc. Natl Acad. Sci. USA 95 (3), 876–882.
Tak, S., Jang, J., Lee, K., Ye, J., 2010. Quantification of $CMRO_2$ without hypercapnia using simultaneous near infrared spectroscopy and fMRI measurements. Phys. Med. Biol. 55, 3249–3269.
Tibshirani, R., 1996. Regression shrinkage and selection via the lasso. J. R. Stat. Soc. B 58 (1), 267–288.
Tohgi, H., Chiba, K., Sasaki, K., Hiroi, S., Ishibashi, Y., 1991. Cerebral perfusion patterns in vascular dementia of Binswanger type compared with senile dementia of Alzheimer type: a SPECT study. J. Neurol. 238 (7), 365–370.
Torricelli, A., Pifferi, A., Taroni, P., Giambattistelli, E., Cubeddu, R., 2001. In vivo optical characterization of human tissues from 610 to 1010 nm by time-resolved reflectance spectroscopy. Phys. Med. Biol. 46 (8), 2227–2238.
Villringer, A., Chance, B., 1997. Non-invasive optical spectroscopy and imaging of human brain function. Trends Neurosci. 20 (10), 435–442.
Wu, G., Luo, F., Li, Z., Zhao, X., Li, S., 2002. Transient relationships among BOLD, CBV, and CBF changes in rat brain as detected by functional MRI. Magn. Reson. Med. 48 (6), 987–993.
Yang, D., Kim, B., Park, J., Kim, S., Kim, E., Sohn, H., 2002. Analysis of cerebral blood flow of subcortical vascular dementia with single photon emission computed tomography: adaptation of statistical parametric mapping. J. Neurol. Sci. 203, 199–205.
Yao, H., Sadoshima, S., Kuwabara, Y., Ichiya, Y., Fujishima, M., 1990. Cerebral blood flow and oxygen metabolism in patients with vascular dementia of the Binswanger type. Stroke 21 (12), 1694–1699.
Ye, J., Tak, S., Jang, K., Jung, J., Jang, J., 2009. NIRS-SPM: statistical parametric mapping for near-infrared spectroscopy. Neuroimage 44, 428–447.
Yoshikawa, T., Murase, K., Oku, N., Kitagawa, K., Imaizumi, M., Takasawa, M., Nishikawa, T., Matsumoto, M., Hatazawa, J., Hori, M., 2003. Statistical image analysis of cerebral blood flow in vascular dementia with small-vessel disease. J. Nucl. Med. 44 (4), 505–511.